IEEE Access
Multidisciplinary | Rapid Review | Open Access Journal

Received August 2, 2020, accepted August 27, 2020, date of publication August 31, 2020, date of current version September 11, 2020.

Digital Object Identifier 10.1109/ACCESS.2020.3020500

Standard Condition Number Based Spectrum Sensing Under Asynchronous Primary User Activity

AMOR NAFKHA, (Senior Member, IEEE)
SCEE/IETR, CentraleSupélec, 35576 Cesson Sévigné, France
e-mail: amor.nafkha@centralesupelec.fr

This work was supported by internal funding from CentraleSupélec.

ABSTRACT Cognitive radio (CR) is a promising technology which enables the secondary user (SU) to sense and detect the presence or absence of the primary user (PU) in the frequency band of interest. Therefore, high detection probability is needed to ensure that primary user is adequately protected, while low false-alarm probability provides the opportunity of using free channel and a better throughput performance of secondary user. Most of the studies on spectrum sensing techniques were conducted assuming a perfect synchronization between the secondary and the primary users. However, in practice, the synchronous assumption is very hard to satisfy in the context of real cognitive radio networks environment. In this paper, we present a theoretical formulation of the standard condition number (SCN) based spectrum sensing technique under an asynchronous cognitive radio networks. We assume the case where the primary users generate asynchronous slotted traffic. The standard condition number distributions under null and alternative hypotheses are derived where the secondary user is equipped with two receive antennas. Under asynchronous primary user traffic, we establish the existence of a lower limit of the false-alarm probability below which we are unable to derive a decision threshold for the SCN-based detector.

INDEX TERMS Spectrum sensing, Markov process, standard condition number, detection probability, false-alarm probability, asynchronous/synchronous traffic.

I. INTRODUCTION

Due to the under-utilization problem of frequency spectrum, the concept of cognitive radio system has been developed as a reliable and effective solution [1]. The cognitive radio exploited unoccupied frequency bands owned by primary (*i.e* licensed) users. In order to benefit from the unused parts of the spectrum, a secondary (*i.e* unlicensed) user needs to monitor it to determine which portions are being unused by the primary user. Sensing an unused frequency band is a difficult task due to noise uncertainty, noise correlation, and the unknown primary user traffic.

Several spectrum sensing techniques like matched filter detector, energy detector, cyclostationary feature detector, high-order statistics based detector, covariance-based detector, and eigenvalue-based detector have been proposed and discussed in terms of their complexity-performance trade-offs in literature [2]–[4]. The energy detector (ED) is a non-coherent, blind and optimal detector for independent and identically distributed signal samples. It gives good detection performance with low computational complexity. However, ED is limited by its dependency on noise uncertainty [5]. Multiple antenna techniques currently are used in communications and their effectiveness has been proven in several aspects. In the context of cognitive radio, multiple antenna at the secondary user can effectively enhance signal transmission and spectrum sensing. Multiple antenna spectrum sensing can improve the primary user detection performance by exploring the spatial diversity [6], [7].

In most studies in literature, spectrum sensing is carried out when the behaviour of primary user remains constant either absent or present during the entire sensing time. This constraint implies that the secondary user and the primary user must be perfectly synchronized which may be difficult to achieve particularly in very low signal to noise ratio regimes. Recently, there have been several works which address the

The associate editor coordinating the review of this manuscript and approving it for publication was Wei Feng.

effect of unknown primary user traffic patterns on the spectrum sensing [8]–[11]. Due to timing misalignment of the primary signal, the primary user may arrive or leave the licensed band at any time during the secondary user sensing time. In fact, this scenario appears when the primary user network has a high traffic rate or when a short secondary frame interval is used. In [10], authors address the sensing performance of energy detector against the random arrival and departure of primary user, while [11] study the effect of a single primary user traffic on secondary user's sensing performance as well as on the throughput. In [8] authors study the effect of multiple primary users traffic on the joint sensing-throughput performance of secondary user. In [9], the authors investigate the performance of the largest eigenvalue based detector under an unknown primary user traffic scenario, and where the secondary user is equipped with multiple receive antennas. They show that the performance gain due the spatial diversity is significantly reduced by the effect of a high transition probability of the primary user traffic.

To the best of authors' knowledge, the performance of standard condition number based spectrum sensing with unknown primary user traffic has not been investigated in the literature, partially due to the difficulty of deriving a simple closed-form expression of the probability density function of standard condition number in finite dimension. Our study is of real interest for two reasons. First, the used standard condition number detector is an efficient spectrum sensing technique in multi-dimensional cognitive radio systems since no a priori knowledge is needed. In fact, in contrast to energy detector and largest eigenvalue based detector, the standard condition number based detector is robust against noise uncertainty. Secondly, the SCN based detector is particularly cost-effective, which makes it a great tool for embedded cognitive receivers. In this paper, we consider a scenario where secondary user is equipped with two antennas and performs spectrum sensing under Rayleigh flat fading channels. The main contributions of this paper are as follows: **(i)** Under asynchronous scenario and unknown primary user activities, we derive new analytical expressions for the cumulative distribution function and probability density function of the SCN random variable. Moreover, we give the closed form expressions of detection and false alarm probabilities. **(ii)** The probability density function of the SCN significantly changes with increasing the mean number of samples received before transition from null to alternative hypothesis and vice versa during the sensing interval. **(iii)** Under asynchronous PU traffic, we establish the existence of the false-alarm probability wall, $P_{fa}^{Asy,wall}$, and we derive its analytic expression.

The remainder of this paper is organized as follows: In Section II, we describe the system model, and we derive mathematical expressions of SCN probability density functions for null and alternative hypotheses under synchronous and asynchronous PU traffic. Matlab simulations and performances analysis under synchronous and asynchronous primary user are provided to validate the accuracy of the derived expressions in Section III. Moreover, we establish the existence of the false-alarm probability wall under asynchronous PU traffic scenario. Finally, Section IV concludes the paper.

Notations: $\mathcal{CN}(0,\sigma^2)$ represents the complex Gaussian distribution with zero mean and σ^2 variance. $\mathbf{I}_x$ means the identity matrix of order x. $\mathbb{E}_x[.]$ denotes the expectation with respect to the random variable x. $\Gamma(.)$ defines the Gamma function as referred in [17, eq. 8.310.1], ${}_1F_1(.)$ is the confluent hypergeometric function as defined in [17, eq. 9.210.1], and ${}_2F_1(.)$ denotes the Gauss hypergeometric function as given in [17, eq. 9.14.2]. χ^2_{2N} represents a central chi-square distribution with $2N$ degrees of freedom and $\chi^2_{2N}(c)$ represents a non-central chi-square distribution with $2N$ degrees of freedom and a non-centrality parameter c.

II. SYSTEM MODEL AND THEORETICAL DERIVATIONS

To theoretically derive the impact of the traffic behavior of primary user on the SCN-based spectrum sensing detector. We start by analytically deriving the probability density functions of the SCN of the received covariance matrix when the time is slotted in both primary and secondary networks and slots of secondary network are synchronous to the primary network. Then, we derive the distributions of SCN of the received covariance matrix when the primary network and the secondary network are not aligned in their timing (*i.e.* asynchronous behavior).

A. SYNCHRONOUS SCN-BASED SPECTRUM SENSING

Let us consider a single secondary user equipped with two uncorrelated receive antennas which is aiming to detect the presence/absence of a single primary user during a sensing time τ_s. During this sensing interval, each of two antennas in secondary user receives N samples (*i.e.* $\tau_s = N/F_s$, where F_s is the sampling frequency). We model the spectrum sensing problem under a synchronous PU traffic, where the PU did not randomly appear or disappear during the sensing time, as a binary hypothesis testing problem: Given the received signal during τ_s, a decision is to be made between the null hypothesis $\mathcal{H}_0$ (*i.e. absence of a PU*) and the alternative hypothesis $\mathcal{H}_1$ (*i.e. presence of a PU*). Then, the received vector $\boldsymbol{y}$ at given instant $n \in [1, 2, \ldots, N]$ can be written, under both hypothesis, as:

$$\begin{cases} \mathcal{H}_0: & \boldsymbol{y}(n) = \boldsymbol{\eta}(n) \\ \mathcal{H}_1: & \boldsymbol{y}(n) = \boldsymbol{h}(n)\boldsymbol{s}(n) + \boldsymbol{\eta}(n). \end{cases} \tag{1}$$

where $\boldsymbol{\eta}(n)$ is a 2×1 complex circular white Gaussian noise, $\boldsymbol{h}(n)$ is a 2×1 complex vector that represents the channel's coefficient between the PU and each antenna at the cognitive radio receiver, modelled like a flat channel as a complex additive white Gaussian noise (AWGN), and $\boldsymbol{s}(n)$ stands for the primary user signal to be detected. After collection N sample at each antenna, the received signal matrix can be

written as:

$$\mathbf{Y} = \begin{pmatrix} y_1(1) & y_1(2) & \dots & y_1(n) \\ y_2(1) & y_2(2) & \dots & y_2(n) \end{pmatrix}, \quad (2)$$

and we define the received samples covariance matrix as: $\mathbf{W} = \frac{1}{2}\mathbf{Y}\mathbf{Y}^H$, where $(.)^H$ denotes the Hermitian complex conjugate. According to binary hypothesis testing, the covariance matrix $\mathbf{W}$ follows the Wishart distribution with two dimension and N degrees of freedom ($i.e. \mathbf{W} \sim \mathcal{CW}_2(N, \Sigma)$). Under the $\mathcal{H}_0$ null hypothesis, the covariance matrix $\mathbf{W}$ follows an uncorrelated central Wishart distribution. However, under the $\mathcal{H}_1$ hypothesis, the covariance matrix $\mathbf{W}$ follows an uncorrelated non-central Wishart distribution.

$$\begin{cases} \mathcal{H}_0 : & \mathbf{W} \sim \mathcal{CW}_2(N, \mathbf{I}_2) \\ \mathcal{H}_1 : & \mathbf{W} \sim \mathcal{CW}_2(N, \mathbf{I}_2, \Omega_2). \end{cases} \quad (3)$$

where $\Omega_2 = \mathbf{Z}\mathbf{Z}^H$ is called non-centrality matrix, with $\mathbf{Z} = [\boldsymbol{h}(1)\boldsymbol{s}(1), \dots, \boldsymbol{h}(N)\boldsymbol{s}(N)]$.

Let's consider the SCN-based statistic for decision process. The SCN-based spectrum sensing technique is a blind detector that uses the eigenvalues of the covariance matrix $\mathbf{W}$. Denoting by $\lambda_1 \geq \lambda_2 > 0$, the ordered eigenvalues of $\mathbf{W}$, the SCN is defined as the ratio of the largest to the smallest eigenvalue of the covariance matrix as follows: $\kappa = \frac{\lambda_1}{\lambda_2}$. In order to make decisions about the hypothesis ($\mathcal{H}_0$ or $\mathcal{H}_1$), we need to derive the distribution of the statistical metric, κ, under null and alternative hypotheses.

Theorem 1: Let $\kappa_N^{\mathcal{H}_0}$ be the SCN associated to the dual complex uncorrelated central Wishart matrix $\mathbf{W} \sim \mathcal{CW}_2(N, \mathbf{I}_2)$ with an arbitrary N, then the PDF and the CDF of $\kappa_N^{\mathcal{H}_0}$ can be expressed, respectively, as

$$f_{\kappa_N^{\mathcal{H}_0}}(x) = \frac{8\Gamma(N+\frac{1}{2})(x-1)^2(4x)^{N-2}}{\sqrt{\pi}\Gamma(N-1)(x+1)^{2N}}; \quad x \in [1, +\infty[\quad (4)$$

and

$$F_{\kappa_N^{\mathcal{H}_0}}(x) = \frac{N(1-x) + 2\left[{}_2F_1(1, -N, N, -x) - 1\right]}{(4x)^{1-N}(1+x)^{2N-1}} \times \frac{2\Gamma(N+\frac{1}{2})}{\sqrt{\pi}\Gamma(N+1)} - 1; \quad x \in [1, +\infty[\quad (5)$$

Proof: Under null hypothesis $\mathcal{H}_0$, the sample covariance matrix $\boldsymbol{W}$ follows a dual uncorrelated complex central Wishart distribution $\mathcal{CW}_2(N, \boldsymbol{I}_2)$. Let's $X = \kappa_N^{\mathcal{H}_0} = \lambda_1/\lambda_2$ be the standard condition number of $\boldsymbol{W}$. Then, using the characteristic polynomial of $\boldsymbol{W}$, we can express the standard condition number x as following

$$x = \frac{1 + \sqrt{1 - 4D/T^2}}{1 - \sqrt{1 - 4D/T^2}} \quad (6)$$

where D and T denote the determinant and the trace of the received covariance matrix $\mathbf{W}$, respectively. The exact probability density function of the random variable $A = 4D/T^2$ can be found in [13]. Making a change of variable A to $U = \sqrt{1-A}$ with Jacobian $J = 2u$, the probability density of U reads

$$f_U(u) = \frac{4\Gamma(N+\frac{1}{2})u^2(1-u^2)^{N-2}}{\sqrt{\pi}\Gamma(N-1)}; \quad u \in [0, 1] \quad (7)$$

Let X be the random variable defined as $X = \Phi(U) = \frac{1+U}{1-U}$. The function Φ is increasing for all U. Then, we can find the inverse function Φ^{-1} as follows:

$$u = \frac{x-1}{x+1} = \Phi^{-1}(x), \quad x \in [1, +\infty[\quad (8)$$

We can then find the derivative of Φ^{-1} with respect to x as

$$\frac{d\Phi^{-1}(x)}{dx} = \frac{2}{(x+1)^2} \quad (9)$$

Finally, the probability density of the standard condition number X can be expressed as:

$$\begin{aligned} f_X(x) &= f_U[\Phi^{-1}(x)] \quad . \quad |\frac{d\Phi^{-1}(x)}{dx}| \\ &= \frac{8\Gamma(N+\frac{1}{2})(x-1)^2(4x)^{N-2}}{\sqrt{\pi}\Gamma(N-1)(x+1)^{2N}}, \end{aligned} \quad (10)$$

where $x \in [1, +\infty[$. The cumulative distribution function of the standard condition number under null hypothesis $\mathcal{H}_0$ can be obtained by integrating the PDF of X. Thus, the CDF of X can be given as

$$F_X(x) = \frac{N(1-x) + 2\left[{}_2F_1(1, -N, N, -x) - 1\right]}{(4x)^{1-N}(1+x)^{2N-1}} \times \frac{2\Gamma(N+\frac{1}{2})}{\sqrt{\pi}\Gamma(N+1)} - 1 \quad (11)$$

We notice that the distribution density of the SCN under null hypothesis, $\kappa_N^{\mathcal{H}_0}$, only depends on the number of received samples N. Finally, the theorem 1 is proved. ■

Likewise, we introduce the following theorem which gives the exact probability density function of the standard condition number under the alternative hypothesis $\mathcal{H}_1$.

Theorem 2: Let $\kappa_{N,\omega_1}^{\mathcal{H}_1}$ be the SCN associated to the dual complex uncorrelated non-central Wishart matrix $\mathbf{W} \sim \mathcal{CW}_2(N, \mathbf{I}_2, \Omega_2)$ with an arbitrary N and rank one matrix Ω_2, then the PDF of $\kappa_{N,\omega_1}^{\mathcal{H}_1}$ is expressed as

$$\begin{aligned} f_{\kappa_{N,\omega_1}^{\mathcal{H}_1}}(x) = \frac{2\Gamma(2N-1)(x-1)x^{N-2}e^{\frac{-\omega_1}{2}}}{\omega_1\Gamma(N-1)^2(x+1)^{2N-1}} \\ \times[{}_1F_1(2N-1, N-1, \frac{\omega_1 x}{2(x+1)}) \\ - {}_1F_1(2N-1, N-1, \frac{\omega_1}{2(x+1)})] \end{aligned} \quad (12)$$

where $\omega_1 = 2\rho N$ is non-zero eigenvalue of the non-centrality matrix Ω_2. The signal to noise ratio is defined by $\rho = \mathbb{E}_h\left[||\boldsymbol{hs}||^2\right]/\mathbb{E}_\eta\left[||\boldsymbol{\eta}||^2\right]$.

Proof: Let's denote by $x = \kappa_{\mathbf{W}}^{\mathcal{H}_1}$ the standard condition number of the dual complex uncorrelated central Wishart matrix $\boldsymbol{W} \sim \mathcal{CW}_2(N, \boldsymbol{I}_2, \boldsymbol{\Omega}_2)$, with ω_1 and ω_2 the eigenvalues of the non-centrality matrix $\boldsymbol{\Omega}_2$. For the rank one

matrix $\mathbf{\Omega}_2$, they are readily given as $\omega_1 = 2\rho N \neq 0$, ρ is the signal-to-noise ratio, while $\omega_2 = 0$. The rank one matrix assumption is justified by the fact that there is at most one primary user. Using the generalized Bartlett's decomposition when the non-centrality matrix $\mathbf{\Omega}_2$ has rank one [18, Th. 10.3.8], Then, let the Cholesky decomposition of $\boldsymbol{W}$ be $\boldsymbol{W} = \boldsymbol{Q}\boldsymbol{Q}^H$,where the lower triangular matrix $\boldsymbol{Q}$ has real positive entries $\boldsymbol{q}_{ii}$ on the diagonal. The entries $\boldsymbol{q}_{ij}$ of $\boldsymbol{Q}$ are all statistically independent and their distributions as follows:

$$\begin{cases} \boldsymbol{q}_{11}^2 \sim \chi_{2N}^2(\omega_1) \\ \boldsymbol{q}_{22}^2 \sim \chi_{2N-2}^2 \\ \boldsymbol{q}_{21}^2 \sim \chi_2^2. \end{cases} \tag{13}$$

Since $\boldsymbol{W} = \boldsymbol{Q}\boldsymbol{Q}^H$, we have

$$\begin{cases} T = \mathrm{tr}(\boldsymbol{W}) = \mathrm{tr}(\boldsymbol{Q}\boldsymbol{Q}^H) = \sum_{i\leq j}^{2} \boldsymbol{q}_{ij}^2 \\ D = \det(\boldsymbol{W}) = \prod_{i=1}^{2} \boldsymbol{q}_{ii}^2. \end{cases} \tag{14}$$

The first step of the proof is to derive the probability density function of the random variable $A = \frac{4D}{T^2}$. By applying a change of variables as follows

$$A = \frac{4\boldsymbol{q}_{11}^2\boldsymbol{q}_{22}^2}{(\boldsymbol{q}_{11}+\boldsymbol{q}_{22}+\boldsymbol{q}_{12})^2} \tag{15}$$

$$X_1 = \boldsymbol{q}_{11} \tag{16}$$

$$X_2 = \boldsymbol{q}_{22} \tag{17}$$

we can derive the joint distribution function of random variables A, X_1, and X_2 as

$$f_{A,X_1,X_2}(a,x_1,x_2) = \frac{x_1^{N-1}x_2^{N-2}\sqrt{\frac{x_1x_2}{a}}e^{-\sqrt{\frac{x_1x_2}{a}}}}{2^{2N}\Gamma(N)\Gamma(N-1)a} \times e^{-\frac{\omega_1}{2}}{}_0F_1(N,\frac{\omega_1x_1}{4}) \tag{18}$$

where ${}_0F_1(\mu,x) = \sum_{j=0}^{+\infty}\frac{\Gamma(\mu)}{\Gamma(\mu+j)}\frac{x^j}{j!}$. Since we are interested in a only, $x_1 \in [0,+\infty[$ and $x_2 \in [\frac{x_1}{a}(1-\sqrt{1-a})^2, \frac{x_1}{a}(1+\sqrt{1-a})^2]$ are integrated out of the above expression; the following result is then the marginal probability density function corresponding to a:

$$f_A(a) = \frac{2\Gamma(2N-1)a^{N-2}e^{\frac{-\omega_1}{2}}}{\omega_1\Gamma(N-1)^2 4^{N-1}} \times[{}_1F_1(2N-1,N-1,\omega_1\frac{1+\sqrt{1-a)}}{4}) - {}_1F_1(2N-1,N-1,\omega_1\frac{1-\sqrt{1-a)}}{4})]; \tag{19}$$

where $a \in [0,1]$. The above equation completes the first step of the proof. Then, similar to proof of Theorem 1, we now proceed with the second step of the proof. Making a change of variable A to $X = \frac{1+\sqrt{1-A}}{1-\sqrt{1-A}}$ with Jacobian $J = \frac{4(x-1)}{(x+1)^3}$, the probability density function of the condition number under alternative hypothesis $\mathcal{H}_1$ reads

$$f_{\kappa_{N,\omega_1}|\mathcal{H}_1}(x) = \frac{2\Gamma(2N-1)(x-1)x^{N-2}e^{\frac{-\omega_1}{2}}}{\omega_1\Gamma(N-1)^2(x+1)^{2N-1}} \times[{}_1F_1(2N-1,N-1,\frac{\omega_1 x}{2(x+1)}) - {}_1F_1(2N-1,N-1,\frac{\omega_1}{2(x+1)})]; \tag{20}$$

where $x \in [1,+\infty[$. Finally, we obtain the desired result. ■

B. ASYNCHRONOUS SCN-BASED SPECTRUM SENSING

We consider here that the gathered samples can follow a mixture of the null and alternative hypotheses. We will rely on a model of the primary user traffic proposed in [9]. In the sequel, the traffic behavior of primary user is modeled by a two-state Markov process (or binary Markov process) as shown in Fig. 1. The first state is the busy state when the primary user is emitting a signal whereas the second state is the idle state when the primary user is absent. We denote by α the probability of going from idle to busy state, and β the probability of going from busy to idle state.

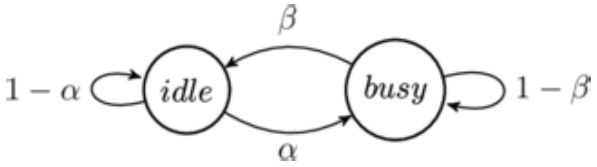

FIGURE 1. Markov chain representing the transitions between idle and busy states.

Then, we can express the mean length of idle and busy periods as, respectively, $M_i = 1/\alpha$ and $M_b = 1/\beta$. For simplicity, we assume that there is at most one state transition during the sensing time τ_s. This is backed up by the fact that, for usual mean length of idle and busy state and length of sensing interval, the probability of observing more than one transition is very small. Fig. 2 shows that as soon as the number of received samples N becomes greater than 20, the probability of having at most one transition becomes close to one and stable when $M = M_i = M_b$ is greater than N. Interested readers can refer to [14]–[16] for more details.

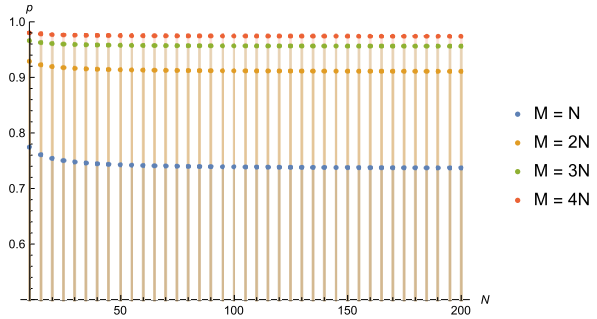

FIGURE 2. Probability of having at most one transition during the sensing time as function of the number of received samples *N*.

For the asynchronous primary user traffic model, we change the definitions of $\mathcal{H}_0$ and $\mathcal{H}_1$ slightly as presented in table 1.

Denoting by steady state (SS) the situation when the received matrix entries come from the same primary user's

TABLE 1. Hypothesis definitions under asynchronous PU traffic.

$SS \mid \mathcal{H}_0$	All received samples are collected during the $idle$ state.
$TS \mid \mathcal{H}_0$	The first received samples are collected during the $busy$ state and the last received sample belongs the $idle$ state.
$SS \mid \mathcal{H}_1$	All received samples are collected during the $busy$ state.
$TS \mid \mathcal{H}_1$	The first received samples are collected during the $idle$ state and the last received sample belongs the $busy$ state.

state (*i.e* idle or busy), and transient state (TS) the situation where the entries of received matrix are a mix between primary user's states.

Theorem 3: The probabilities that all received samples belong to the same steady state ($\mathcal{H}_0$ resp. $\mathcal{H}_1$) are given by

$$P_{SS|\mathcal{H}_0} = \frac{1}{1+\alpha\sum_{d=1}^{N}\frac{(1-\beta)^{N-d-1}}{(1-\alpha)^{N-d}}} \tag{21}$$

$$P_{SS|\mathcal{H}_1} = \frac{1}{1+\beta\sum_{d=1}^{N}\frac{(1-\alpha)^{N-d-1}}{(1-\beta)^{N-d}}} \tag{22}$$

Proof: Let $P_i = \frac{M_i}{M_i+M_b}$ and $P_b = \frac{M_b}{M_i+M_b}$ denote the probability of a sample being from a idle and busy states, respectively. Then, the joint probability mass of having no transition event and a idle state is written as:

$$P(SS, \mathcal{H}_0) = P_i(1-\alpha)^N \tag{23}$$

Similarly, the joint probability mass of having a transition from $\mathcal{H}_1$ to $\mathcal{H}_0$ and the $\mathcal{H}_0$ state is given by

$$P(TS, \mathcal{H}_0) = P_b\sum_{d=1}^{N-1}(1-\beta)^{N-d-1}\beta(1-\alpha)^d \tag{24}$$

Consequently, we obtain:

$$\begin{aligned} P_{SS|\mathcal{H}_0} &= \frac{P(SS,\mathcal{H}_0)}{P(SS,\mathcal{H}_0)+P(TS,\mathcal{H}_0)} \\ &= \frac{1}{1+\alpha\sum_{d=1}^{N}(1-\beta)^{N-d-1}(1-\alpha)^{d-N}} \end{aligned} \tag{25}$$

For $P_{SS|\mathcal{H}_1}$, a similar reasoning yields:

$$\begin{aligned} P_{SS|\mathcal{H}_1} &= \frac{P(SS,\mathcal{H}_1)}{P(SS,\mathcal{H}_1)+P(TS,\mathcal{H}_1)} \\ &= \frac{1}{1+\beta\sum_{d=1}^{N}(1-\alpha)^{N-d-1}(1-\beta)^{d-N}} \end{aligned} \tag{26}$$

■

From the equations (21) and (22), we can note that if M_i and M_b are equal to a given value M, (*i.e* $\alpha = \beta$), then $P_{SS|\mathcal{H}_0} = P_{SS|\mathcal{H}_1} = \frac{M}{M+N}$.

In order to study the transient states, we depict the timing misalignment among PU and SU in Fig. 3. Let us define two random variables: D_0, the number of received samples belonging the null hypothesis $\mathcal{H}_0$ during a transition from busy state to idle state, and D_1, the number of received samples belonging the alternative hypothesis $\mathcal{H}_1$ during a transition from idle state to busy state.

Theorem 4: The probabilities of receiving d_0 (*resp.* d_1) samples belonging the null hypothesis $\mathcal{H}_0$ (*resp.* the alternative hypothesis $\mathcal{H}_1$) during a transition from busy to idle state (*resp.* from idle to busy state) are given respectively by:

$$P_{D_0}(d_0) = \frac{(1-\beta)^{N-d_0-1}(1-\alpha)^{d_0-N}}{\sum_{d=1}^{N-1}(1-\beta)^{N-d-1}(1-\alpha)^{d-N}} \tag{27}$$

$$P_{D_1}(d_1) = \frac{(1-\alpha)^{N-d_1-1}(1-\beta)^{d_1-N}}{\sum_{d=1}^{N-1}(1-\alpha)^{N-d-1}(1-\beta)^{d-N}} \tag{28}$$

Proof: During a transient state from a busy to a idle state, the probability to have d_0 samples belonging to a null hypothesis $\mathcal{H}_0$ is given by:

$$P(TS, d_0, \mathcal{H}_0) = P_b(1-\beta)^{N-d_0-1}\beta(1-\alpha)^{d_0} \tag{29}$$

where $P_b = \frac{M_b}{M_i+M_b}$. As a consequence, the probability of receiving d_0 samples belonging the null hypothesis $\mathcal{H}_0$ during a transition from busy to idle state can be expressed as:

$$\begin{aligned} P_{D_0}(d_0) &= \frac{P(TS,d_0,\mathcal{H}_0)}{\sum_{d=1}^{N-1}P(TS,d,\mathcal{H}_0)} \\ &= \frac{(1-\beta)^{N-d_0-1}(1-\alpha)^{d_0-N}}{\sum_{d=1}^{N-1}(1-\beta)^{N-d-1}(1-\alpha)^{d-N}} \end{aligned} \tag{30}$$

Similarly, we derive $P_{D_1}(d_1)$ as

$$\begin{aligned} P_{D_1}(d_1) &= \frac{P(TS,d_1,\mathcal{H}_1)}{\sum_{d=1}^{N-1}P(TS,d,\mathcal{H}_1)} \\ &= \frac{(1-\alpha)^{N-d_1-1}(1-\beta)^{d_1-N}}{\sum_{d=1}^{N-1}(1-\alpha)^{N-d-1}(1-\beta)^{d-N}} \end{aligned} \tag{31}$$

■

From equations (27) and (28), we can denote that if M_i is equal to M_b, then the analytical expression of $P_{D_0}(d_0)$ and $P_{D_1}(d_1)$ can be reduced to: $P_{D_0}(d_0) = P_{D_1}(d_1) = \frac{1}{N-1}$, with $1 \leq d_0, d_1 < N$.

C. SCN DISTRIBUTIONS UNDER AN ASYNCHRONOUS PU TRAFFIC

Before deriving the distributions of the SCN under an asynchronous primary user traffic, the notations of several probability density functions are defined for clarity and understanding in table 2.

Using the fact that $f^{TS}_{\mathcal{H}_0,d} = f^{TS}_{\mathcal{H}_1,N-d}$, we can write the probability density functions, for a transient state (from busy to idle state, or vice versa) with unknown number of received samples coming from a busy state, as:

$$f^{TS}_{\mathcal{H}_0} = \sum_{d=1}^{N-1}P_{D_0}(d)f^{TS}_{\mathcal{H}_1,N-d} \tag{32}$$

$$f^{TS}_{\mathcal{H}_1} = \sum_{d=1}^{N-1}P_{D_1}(d)f^{TS}_{\mathcal{H}_1,d} \tag{33}$$

Consequently, we are able to derive the probability density function of the SCN under the null hypothesis $\mathcal{H}_0$ (resp. alternative hypothesis $\mathcal{H}_1$), given the considered asynchronous

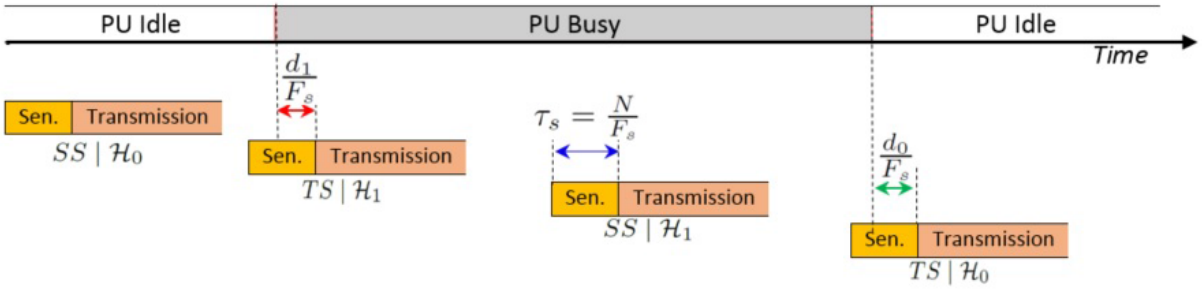

FIGURE 3. Timing misalignment model for four traffic patterns. The PU is slotted, whereas the SU is asynchronous to the PU. τ_S is the sensing time and F_S is the sampling frequency at the secondary user receiver.

TABLE 2. Probability density functions under transient and steady states.

$f^{SS}_{\mathcal{H}_0} = f_{\kappa_N \mid \mathcal{H}_0}$	Probability density function of the SCN when the N received samples belong idle state.
$f^{SS}_{\mathcal{H}_1} = f_{\kappa_{N,2\rho N} \mid \mathcal{H}_1}$	Probability density function of the SCN when the N received samples belong busy state.
$f^{TS}_{\mathcal{H}_0,d} = f_{\kappa_{N,2\rho(N-d)} \mid \mathcal{H}_1}$	Probability density function of the SCN for a transient from busy to idle state with d samples belonging the idle state.
$f^{TS}_{\mathcal{H}_1,d} = f_{\kappa_{N,2\rho d} \mid \mathcal{H}_1}$	Probability density function of the SCN for a transient from idle to busy state with d samples belonging the busy state.

PU traffic, as following:

$$f^{Asy}_{\kappa_N \mid \mathcal{H}_0} = P_{SS\mid\mathcal{H}_0} f_{\kappa_N \mid \mathcal{H}_0} + P_{TS\mid\mathcal{H}_0} f^{TS}_{\mathcal{H}_0} \tag{34}$$

$$f^{Asy}_{\kappa_N \mid \mathcal{H}_1} = P_{SS\mid\mathcal{H}_1} f_{\kappa_{N,\omega_1} \mid \mathcal{H}_1} + P_{TS\mid\mathcal{H}_1} f^{TS}_{\mathcal{H}_1} \tag{35}$$

If we assume that $M_i = M_b = M$ $(i.e.\ \alpha = \beta)$, then Eq.(34) and Eq.(35) can be written as follows:

$$f^{Asy}_{\kappa_N \mid \mathcal{H}_0} = \frac{M f_{\kappa_N \mid \mathcal{H}_0} + \frac{N}{N-1} \sum_{d=1}^{N-1} f_{\kappa_{N,2\rho(N-d)} \mid \mathcal{H}_1}}{N+M} \tag{36}$$

$$f^{Asy}_{\kappa_N \mid \mathcal{H}_1} = \frac{M f_{\kappa_{N,2\rho N} \mid \mathcal{H}_1} + \frac{N}{N-1} \sum_{d=1}^{N-1} f_{\kappa_{N,2\rho(N-d)} \mid \mathcal{H}_1}}{N+M} \tag{37}$$

III. PERFORMANCES ANALYSIS UNDER SYNCHRONOUS/ASYNCHRONOUS TRAFFIC

In this section, we analyzed the gap in term of false alarm probability, detection probability, and receiver operating characteristics between the classical synchronous spectrum sensing schema and the asynchronous spectrum sensing schema as described in Section II-B. In the sequel of this paper, for simplicity, we assume that the mean length of idle PU state M_i and busy PU state M_b are equal to a given parameter M.

A. FALSE-ALARM PROBABILITY

Let us denote by λ^{syn} the decision threshold under a synchronous PU traffic, then the false alarm probability P^{Syn}_{fa}, defined as the probability of detecting the presence of primary user while it does not exist, is given by:

$$\begin{aligned} P^{Syn}_{fa} &= Prob(\kappa^{\mathcal{H}_0}_N \geq \lambda^{syn} \mid \mathcal{H}_0) \\ &= 1 - F_{\kappa_N \mid \mathcal{H}_0}(\lambda^{syn}) \end{aligned} \tag{38}$$

where $F_{\kappa_N \mid \mathcal{H}_0}(.)$ is the cumulative distribution function of the standard condition number as defined in equation (5). Since the probability density function of the SCN under $\mathcal{H}_0$ and synchronous traffic only depends on number of received samples N, we can characterize the SCN-based spectrum sensing detector by its detection performance for a fixed false-alarm probability. In order to measure the gap in term of false-alarm probabilities between the classical synchronous and the asynchronous PU traffic sensing, one must use λ^{syn} as a threshold to evaluate the false-alarm probability under the asynchronous scenario. Therefore, we can calculate the false alarm probability under asynchronous scenario as follows:

$$\begin{aligned} P^{Asyn}_{fa} &= \int_{\lambda^{syn}}^{+\infty} f^{Asy}_{\kappa_N \mid \mathcal{H}_0}(t)dt \\ &= \frac{M P^{Syn}_{fa}}{N+M} + \frac{N \sum_{d=1}^{N-1} \Xi^{Asy}(d,N,\rho)}{(N-1)(N+M)} \end{aligned} \tag{39}$$

where $\Xi^{Asy}(d,N,\rho) = \int_{\lambda^{syn}}^{+\infty} f_{\kappa_{N,2\rho(N-d)} \mid \mathcal{H}_1}(t)dt$. It is important to note that the limit of $\Xi^{Asy}(d,N,\rho)$ as ρ approaches zero is P^{Syn}_{fa}.

In Fig. 4, the probability density functions $f_{\kappa_N \mid \mathcal{H}_0}(x)$ and $f^{Asy}_{\kappa_N \mid \mathcal{H}_0}(x)$ are depicted for $N = 128$ and $\alpha = \beta$. Under asynchronous PU traffic the probability density function of the SCN, $f^{Asy}_{\kappa_N \mid \mathcal{H}_0}(x)$, is shown for three different values of the SNR ρ. To quantify the similarity of the distribution of the SCN under the synchronous null hypothesis and the asynchronous one, we use the Hellinger distance [19, Definition 2.3] as a metric to evaluate the difference between the mentioned distributions. The Hellinger distance ranges from 0 to 1, where 1 means that the probability distributions are completely different, however 0 means that two probability distributions are identical. The Hellinger distance values obtained are 0.00255, 0.02144 and 0.07606 corresponding to SNR equal to -6 dB, -3 dB, and 0 dB respectively. Therefore, it is easy to conclude

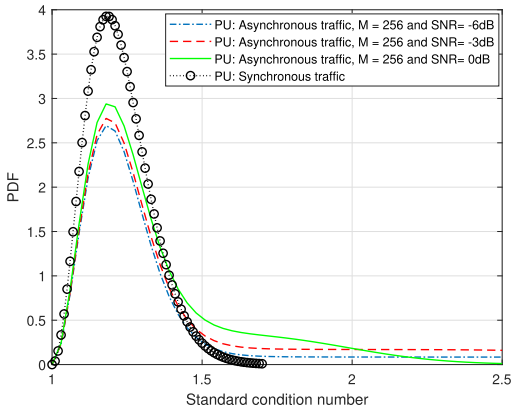

FIGURE 4. PDF under $\mathcal{H}_0$ of the SCN for different values of the SNR and $N = 128$ number of samples.

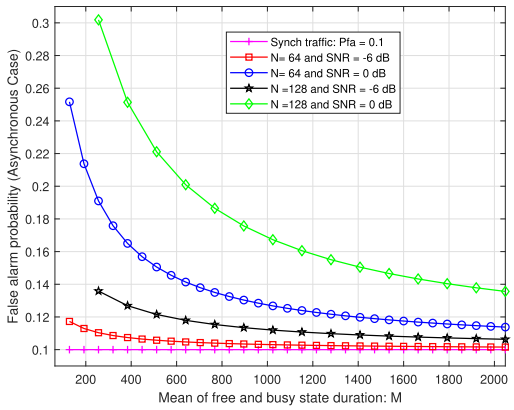

FIGURE 5. False alarm probabilities under Synchronous and Asynchronous PU traffic versus SNR.

that as the SNR tends to minus infinity (no signal), the SCN probability density function $f^{Asy}_{\kappa_N|\mathcal{H}_0}$ converges to $f_{\kappa_N|\mathcal{H}_0}$.

In Fig. 5, we evaluate the effect of the mean length M on the false-alarm probabilities of synchronous and asynchronous scenarios. We can see that the false-alarm probability under asynchronous PU traffic approaches the false-alarm probability under synchronous case as the mean length $M \to \infty$. This can be justified by recalling that the P_{fa}^{Asyn}, derived in (39), is a function of M. As a matter of fact, asymptotically when $M \to +\infty$ and a fixed value of N, the first term tends to P_{fa}^{Syn}, however the second term vanishes and approaches to zero.

Fig. 6 depicts the variation of false-alarm probability under asynchronous PU activity as a function of signal-to-noise ratio in following parameters pairs: $(N = 64, M = 128)$, $(N = 64, M = 256)$, $(N = 128, M = 256)$, and $(N = 128, M = 512)$. Two main observations can be made. First, the false-alarm probability under asynchronous PU traffic converges at low SNR to 0.1, which is the false-alarm probability under synchronous PU traffic. The convergence at low SNR can be explained using (39) by noting that at small SNR value (*i.e* ρ approaches zero), the function $\Xi^{Asy}(d, N, \rho)$ converges to P_{fa}^{Syn}. Second, depends from parameters N and M, the false-alarm probability under asynchronous PU traffic converges to constant values as the signal-to-noise ratio

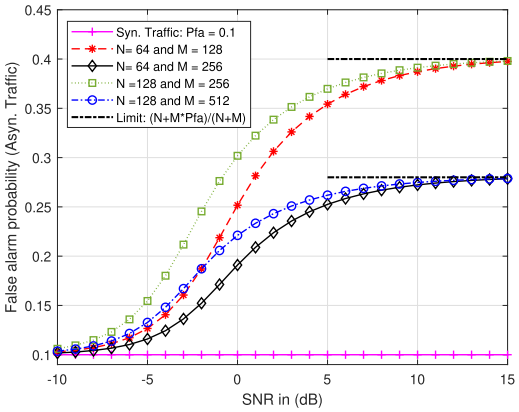

FIGURE 6. False alarm probabilities under Synchronous and Asynchronous PU traffic versus SNR.

increases. Those limits can be deduced from (39) as follows: For high SNR, the function $\Xi^{Asy}(d, N, \rho)$ converges to the unity as $\rho \to +\infty$. Thus, for the high SNR regime, we have the following approximation of P_{fa}^{Asyn} as:

$$P_{fa,wc}^{Asyn} = \lim_{\rho \to \infty} P_{fa}^{Asyn} \approx \frac{N + MP_{fa}^{Syn}}{N + M}, \tag{40}$$

where $P_{fa,wc}^{Asyn}$ denotes the "worst-case" false alarm probability under an asynchronous PU traffic. We can also note that, for fixed SNR and mean length M, the false-alarm probability under asynchronous PU traffic increases as the number of received samples N increases. Intuitively, this can be explained by the fact that, if N increases, the probability that PU is first active at the begin of sensing interval and then becomes idle by the end of the sensing interval or vice-versa, increases.

Fig.7 shows the false-alarm probability under asynchronous PU traffic in worst-case condition, $P_{fa,wc}^{Asyn}$, for different pairs (N,M). The horizontal axis represents the false-alarm probability under synchronous PU traffic P_{fa}^{Syn}. As can be seen in Fig. 7, for a fixed N, as the mean length M increases the false-alarm probability $P_{fa,wc}^{Asyn}$ is improved as the part of the distribution under $\mathcal{H}_0$ to the left of the threshold λ^{syn} increases. Fig. 7 is well-known as probability–probability (P-P) plot tool for the applied statistics. A P-P plot that lies on the first bisector line indicates that the two studied cumulative distributions are identical, whereas a P-P plot lying strictly above the first bisector line, as the case in Fig.7, indicates that $P_{fa,wc}^{Asyn}$ stochastically dominates[1] P_{fa}^{Syn}.

[1]Let X_1 and X_2 two random variables. We say that X_1 first-order stochastically dominates X_2 if and only if $Pr\,(X_1 > c) \geq Pr\,(X_2 > c)$, whatever the value of c.

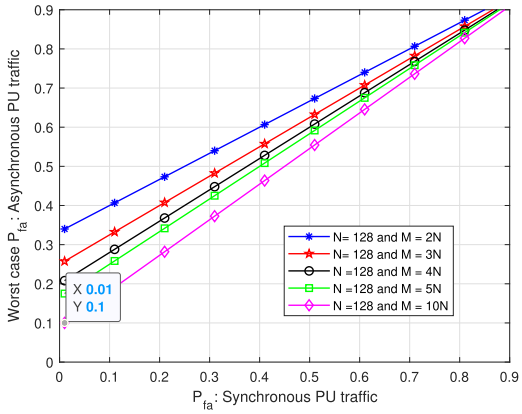

FIGURE 7. Worst case of false-alarm probability under asynchronous PU traffic versus P_{fa}^{Syn}. The graph compares five different pairs (N, M).

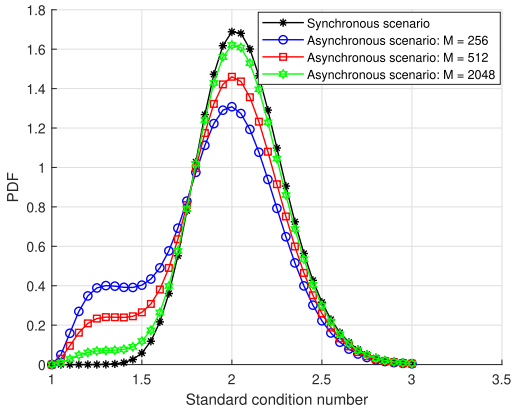

FIGURE 8. Probability density function of the SCN under $\mathcal{H}_1$ as function of M with $N = 128$ and SNR = 0dB.

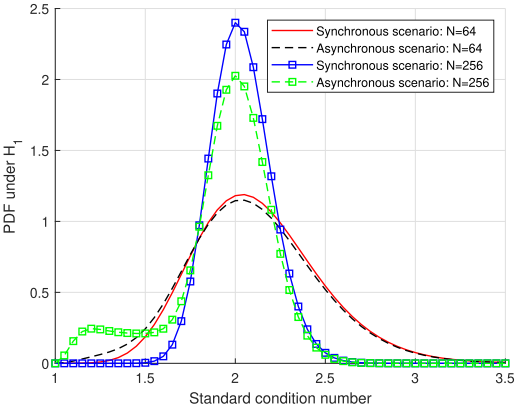

FIGURE 9. Probability density function of the SCN under $\mathcal{H}_1$ as function of N with $M = 1024$ and SNR = 0dB.

B. DETECTION PROBABILITY

In order to guarantee a high reuse probability of the unused spectrum by the secondary user, we adopt the constant false alarm rate (CFAR) based detection criterion. According to the CFAR principle, the probability of false-alarm is fixed to a small value while the detection probability should be maximized. Let us fix the false-alarm probability to a given value γ. Then, the detection probability my be obtained for the two different primary user traffic scenarios. In the case of a synchronous PU traffic, the detection probability is given by

$$P_d^{Syn} = \int_{\lambda^{syn}}^{+\infty} f_{\kappa_{N,\omega_1}}(x)dx \tag{41}$$

where $\lambda^{syn} = F^{-1}_{\kappa_N}(1-\gamma)$. In case of asynchronous PU traffic, the detection probability can be expressed as

$$P_d^{Asyn} = \int_{\lambda^{Asyn}}^{+\infty} f^{Asy}_{\kappa_N}(x)dx \tag{42}$$

where the decision threshold λ^{Asyn} was derived for the worst-case condition as

$$\lambda^{Asyn} = F^{-1}_{\kappa_N}\left((1-\gamma)(1+\frac{N}{M})\right) \tag{43}$$

From (43), it can be seen that the detection threshold under asynchronous PU traffic depends on the pair (N,M). Moreover, given a fixed number of received samples N, λ^{Asyn} converges to λ^{syn} as the mean length M tends to infinity.

Fig. 8 shows the probability density function of the SCN under synchronous and asynchronous primary user traffic with fixed SNR equal to 0 dB, number of received samples $N = 128$, and different values of the the mean length of idle/busy state M. As same as in Fig. 4, the Hellinger distance is used to quantify the similarity between different probability distributions. Given fixed SNR and $N = 128$, the Hellinger distances between $f_{\kappa_{N,2\rho N}}$ and $f^{Asy}_{\kappa_N}$ are quite significant, being 0.0751, 0.0405, and 0.0095 for $M = 256$, $M = 512$ and $M = 2048$, respectively. Moreover, analyzing the expression (37), it can be seen that as M approaches infinity, $f^{Asy}_{\kappa_N}$ approaches $f_{\kappa_{N,2\rho N}}$ due to the fact that the second term tends to zero.

Under both scenarios, the numerically evaluated probability density function of the SCN under $\mathcal{H}_1$ hypothesis, for fixed M and SNR values, as function of the number of received samples N is plotted in Fig. 9. Given fixed SNR and $M = 1024$, the probability density functions curves change slightly between both scenarios when $N = 64$ (i.e. Hellinger distance = 0.0036). However, in the case when $N = 256$, we note that the probability density functions curves are significantly different from each other (i.e. Hellinger distance = 0.0567), which indicates that the detection probabilities values under both scenarios will be very different too. Theoretically, for any N, as the ratio M/N tends to infinity, the probability density function of the SCN under asynchronous scenario converges to $f_{\kappa_{N,2\rho N}}$.

Fig. 10 shows a comparison between the considered two scenarios, asynchronous and synchronous PU traffic, in term of detection probabilities as function of SNR. To keep the performance comparison consistent, we fixed the false-alarm probability target to the value of 0.1 for all graphs (*i.e.* $P_{fa}^{Syn} = P_{fa,wc}^{Asyn} = 0.1$). It is obvious that under synchronous scenario,

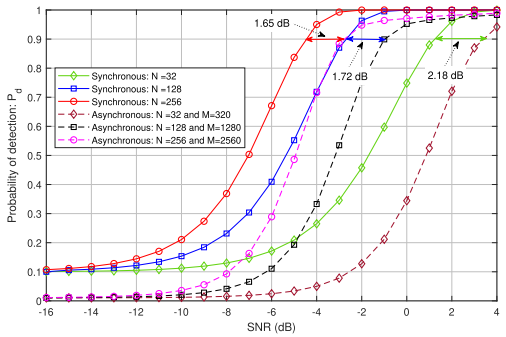

FIGURE 10. Probability of detection versus SNR with target false-alarm probability equal to 0.1, and different (N, M) pairs.

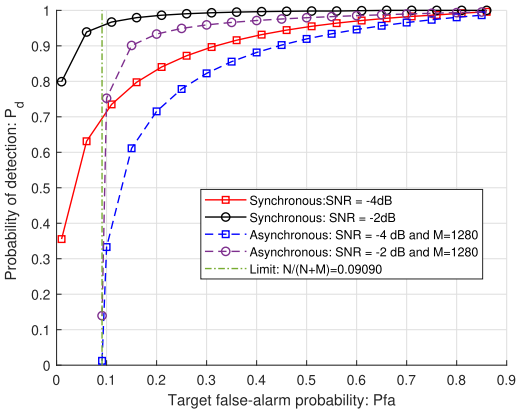

FIGURE 11. The ROC curves for $N = 128$. Solid lines represent different SNR values, -4 dB and -2 dB, under synchronous PU traffic, dashed lines represent different SNR values, -4 dB and -2 dB, under asynchronous PU traffic for fixed $M = 10 \times N$, and dot-dashed line represent the theoretical lower bound of false-alarm probability under asynchronous scenario with $N = 128$ and $M = 1280$.

the SCN-based detector achieves best performances. Moreover, as expected, the detection performance improves with the increase of the number of received samples N during the sensing time. Using (40), we are able to fix the mean duration of primary user busy/idle state M to $10 \times N$ in order to ensure that the target false-alarm probability is at most 0.1 under asynchronous scenario. From Fig. 10, we can see that the detection performance of the SCN-based sensing technique degrades severely under asynchronous PU traffic. Moreover, it can be noted that the SNR gap between synchronous and asynchronous scenarios decreases as M increases. Thus, for a detection probability of 0.9, the SNR gap between the two considered scenarios with $(N = 32, M = 320)$, $(N = 128, M = 1280)$, and $(N = 256, M = 2560)$, is 2.18 dB, 1.72 dB, and 1.65 dB respectively.

C. RECEIVER OPERATING CHARACTERISTIC

The SCN-based detector performance can be represented by the receiver operation characteristic (ROC) curves, in which the detection probabilities and false alarm probabilities are plotted. Thus, the ROC curves indicate the practical regions inside of which the SCN-based detector is capable of providing reliable results. Fig. 11 shows that, for the SCN-based detector over Rayleigh fading channel, ROC curves move to the upper left corner as increasing SNR under any scenarios (synchronous/asynchronous), confirming better overall detection performance. By comparing the results collected in Fig. 11, it is noticeable that the no synchronization between PU and SU during the sensing time decreases the probability of detection for a given false alarm probability. We note that, the main observation is in Fig. 11, which shows the existence of the "P_{fa} *wall*" phenomenon, below which SCN-based detector will fail to be robust under asynchronous scenario. The position of this "P_{fa} *wall*" is determined by N and M, and it can be derived as follows:

$$P_{fa}^{Asy,wall} = \frac{N}{N+M} \tag{44}$$

IV. CONCLUSION

From the view of an opportunistic spectrum access, correct detection of the absence or presence of primary user is a vital component. Traditionally, perfect synchronization between PU and SU is assumed, which is infeasible in the absence of a centralized control unit. In this paper, we discuss the impact of an asynchronous situation, which means SU have no idea about the communication time of PU, on the detection performance of SCN-based technique for spectrum sensing. By assuming that the PU activity follows with an idle/busy Markov chain, we derived the false-alarm and detection probabilities under asynchronous scenario. The existence of the "P_{fa} *wall*" has been established, and its exact expression has been derived. While the present paper considered a single SU and a single primary spectrum band, our main future objective is to extend the presented analytical framework to the case of asynchronous cooperative spectrum sensing where there are no synchronization among the different secondary users, and also between them and the primary user.

ACKNOWLEDGMENT

The author gratefully acknowledges the helpful discussions with Gurvan Priem, an engineer at Biosency company.

REFERENCES

[1] S. Haykin, "Cognitive radio: Brain-empowered wireless communications," *IEEE J. Sel. Areas Commun.*, vol. 23, no. 2, pp. 201–220, Feb. 2005.
[2] T. Yucek and H. Arslan, "A survey of spectrum sensing algorithms for cognitive radio applications," *IEEE Commun. Surveys Tuts.*, vol. 11, no. 1, pp. 116–130, 1st Quart., 2009.
[3] Y. Zeng, Y.-C. Liang, A. T. Hoang, and R. Zhang, "A review on spectrum sensing for cognitive radio: Challenges and solutions," *EURASIP J. Adv. Signal Process.*, vol. 2010, no. 1, pp. 1–15, Dec. 2010.
[4] A. Ali and W. Hamouda, "Advances on spectrum sensing for cognitive radio networks: Theory and applications," *IEEE Commun. Surveys Tuts.*, vol. 19, no. 2, pp. 1277–1304, 2nd Quart., 2017.
[5] R. Tandra and A. Sahai, "SNR walls for signal detection," *IEEE J. Sel. Topics Signal Process.*, vol. 2, no. 1, pp. 4–17, Feb. 2008.
[6] A. Nafkha and B. Aziz, "Closed-form approximation for the performance of finite sample-based energy detection using correlated receiving antennas," *IEEE Wireless Commun. Lett.*, vol. 3, no. 6, pp. 577–580, Dec. 2014.
[7] H. Kobeissi, A. Nafkha, Y. Nasser, Y. Louët, and O. Bazzi, "Approximating the standard condition number for cognitive radio spectrum sensing with finite number of sensors," *IET Signal Process.*, vol. 11, no. 2, pp. 145–154, Apr. 2017.
[8] H. Pradhan, S. S. Kalamkar, and A. Banerjee, "Sensing-throughput tradeoff in cognitive radio with random arrivals and departures of multiple primary users," *IEEE Commun. Lett.*, vol. 19, no. 3, pp. 415–418, Mar. 2015.

[9] P. Dhakal, S. K. Sharma, S. Chatzinotas, B. Ottersten, and D. Riviello, "Effect of primary user traffic on largest eigenvalue based spectrum sensing technique," in *Proc. Int. Conf. Cogn. Radio Oriented Wireless Netw. (CrownCom)*, 2016, pp. 67–78.
[10] I. Atef, A. Eltholth, A. S. Ibrahim, and M. S. El-Soudani, "Energy detection of random arrival and departure of primary user signals in cognitive radio systems," in *Proc. IEEE Int. Conf. Comput. as a Tool (EUROCON)*, Sep. 2015, pp. 1–6.
[11] M. Jin, Q. Guo, Y. Li, J. Xi, and Y. Yu, "Energy detection with random arrival and departure of primary signals: New detector and performance analysis," *IEEE Trans. Veh. Technol.*, vol. 66, no. 11, pp. 10092–10101, Nov. 2017.
[12] A. Zanella, M. Chiani, and M. Z. Win, "On the marginal distribution of the eigenvalues of wishart matrices," *IEEE Trans. Commun.*, vol. 57, no. 4, pp. 1050–1060, Apr. 2009.
[13] D. K. Nagar, S. K. Jain, and A. K. Gupta, "Distribution of LRC for testing sphericity of a complex multivariate Gaussian model," *Int. J. Math. Math. Sci.*, vol. 8, no. 3, pp. 555–562, 1985.
[14] L. T. Tan and L. B. Le, "Distributed MAC protocol design for full-duplex cognitive radio networks," in *Proc. IEEE Global Commun. Conf. (GLOBECOM)*, San Diego, CA, USA, Dec. 2014, pp. 1–6.
[15] C. Fu, Y. Li, Y. He, M. Jin, G. Wang, and P. Lei, "An inter-frame dynamic double-threshold energy detection for spectrum sensing in cognitive radios," *EURASIP J. Wireless Commun. Netw.*, vol. 2017, no. 1, p. 118, Dec. 2017.
[16] M. R. Amini, M. Mahdavi, and M. J. Omidi, "Discrete-time Markov chain analysis of energy efficiency in a CR network regarding primary and secondary traffic with primary user returns," *IEEE Access*, vol. 6, pp. 22305–22323, 2018.
[17] I. S. Gradshteyn and I. M. Ryzhik, *Table of Integral, Series, and Products*, 7th ed. New York, NY, USA: Academic, 2007.
[18] R. J. Muirhead, "Aspects of multivariate statistical theory," in *Wiley Series in Probability and Mathematical Statistics*. New York, NY, USA: Wiley, 1982.
[19] A. B. Tsybakov, *Introduction to Nonparametric Estimation*. New York, NY, USA: Springer, 2009.

AMOR NAFKHA (Senior Member, IEEE) received the B.Sc. (Eng.) degree from the Higher School of Communications (SupCom), Tunis, Tunisia, in 2001, and the Ph.D. degree from the University of South Brittany (UBS), Lorient, France, in 2006, all in information and communications technology. From 2006 to 2007, he was a Postdoctoral Researcher with the Signal, Communication, and Embedded Electronics (SCEE-IETR) Research Group, CentraleSupélec, France. During this time at SCEE, he was actively involved in the reconfigurable hardware platform implementation for software-defined radio, co-authoring several contributions on FPGA dynamic partial reconfiguration. Since January 2008, he has been an Associate Professor at CentraleSupélec. He has published more than 70 papers in international peer-reviewed journals and conferences. His research interests include multiuser and MIMO detection, hardware implementation, information theory, sample rate conversion, and spectrum sensing techniques.